Journal of Molecular Graphics and Modelling 30 (2011) 46–53

Contents lists available at ScienceDirect

Journal of Molecular Graphics and Modelling

journal homepage: www.elsevier.com/locate/JMGM

Insight into mechanism of small molecule inhibitors of the MDM2–p53 interaction: Molecular dynamics simulation and free energy analysis

Jianzhong Chen[a,b], Jinan Wang[c], Beisi Xu[a], Weiliang Zhu[c], Guohui Li[a,*]

[a] Laboratory of Molecular Modeling and Design, State Kay Laboratory of Molecular Reaction Dynamics, Dalian Institute of Chemical Physics, Chinese Academy of Science, 116011, China
[b] Department of Mathematics and Physics, Shandong Jiaotong University, Jinan 250031, China
[c] Drug Discovery and Design Center, Shanghai Institute of Materia Medica, Chinese Academy of Sciences, 555 Zuchongzhi Road, Shanghai 201203, China

ARTICLE INFO

Article history:
Received 3 April 2011
Received in revised form 3 June 2011
Accepted 3 June 2011
Available online 13 June 2011

Keywords:
MDM2–p53 interaction
Cross-correlation analysis
Molecular dynamics simulation
Binding free energy
Hydrophobic interaction

ABSTRACT

Inhibition of the MDM2–p53 interaction is considered to be a new therapeutic strategy to activate wild-type p53 in tumors. Molecular dynamics (MD) simulations followed by molecular mechanics generalized Born surface area (MM-GBSA) analyses were used to study the inhibitory mechanisms of four small molecule inhibitors, K23, YIN, DIZ and IMZ on the p53–MDM2 interaction. We found excellent agreement between the rank of the calculated absolute binding free energies using the MM-GBSA method and the experimentally determined rank. The results show that van der Waals energy is the dominant factor for the binding of the four inhibitors. Statistical analyses of the hydrophobic contacts between the inhibitors and MDM2 were performed, and the results suggested that these inhibitors form stable hydrophobic interactions with six residues of MDM2: Leu54, Gly58, Ile61, Met62, Val93 and His96. Calculations of the detailed van der Waals interactions between non-peptide inhibitors and individual protein residues can provide insights into the inhibitor-protein binding mechanism. Our studies suggest that the CH–π and π–π interactions between the four inhibitors and protein residues drive binding of the inhibitors in the hydrophobic cleft of MDM2.

1. Introduction

The tumor suppressor protein p53 plays a key role in the regulation of the cell cycle, apoptosis, and DNA repair and protects cells from malignant transformation [1–3]. The active form of p53 can effectively suppress oncogenesis. In fact, almost 50% of all human cancers have been shown to have defects in p53 function caused by deletions or mutations in the DNA-binding domain of p53 [4]. However, the activation of p53 is tightly controlled by MDM2, a protein that inhibits the ability of p53 to bind to DNA and activate transcription. Thus, the MDM2–p53 interaction becomes an attractive molecular target for cancer therapy.

p53 interacts with MDM2 by inserting its hydrophobic face (Phe19′, Trp23′, and Leu26′) into a deep groove in MDM2, and direct disruption on the binding of p53 to MDM2 may be an attractive pathway of targeted anticancer therapy [5]. Many peptide inhibitors that mimic the MDM2–p53 interaction have been reported in previous scientific studies [6–8]. Although these peptide inhibitors possess high affinity for MDM2, they display only modest potency in a cellular context, presumably because they have poor membrane permeability [9,10]. Despite the many efforts of academia and the pharmaceutical industry to solve the shortcomings of peptide inhibitors over the past decade, few effective small-molecule inhibitors of the p53–MDM2 interaction are used as clinical therapies [11–13]. The design of potent non-peptide small-molecule inhibitors to target the interaction between p53 and MDM2 has become the current goal for cancer therapy development.

Several different small-molecule inhibitors have been designed by structure-based methods to interrupt the binding of p53 to MDM2. The first type of inhibitor is named the Nutlins, which are based on cis-imidazolidine. The median inhibitory concentration (IC50) values of the Nutlins are in the range of 100–300 nM [1,14]. The second potent antagonists of the MDM2–p53 interaction are a series of benzodiazepinedione derivatives, which inhibit the formation of the MDM2–p53 complex with IC50 values within the range of 7–30 μM [15,16]. The third type of inhibitor is based on spirooxindole and displays potent inhibitory ability and high selectivity for the MDM2–p53 complex [17,18]. Recently, T.A. Holak et al. used a new imidazoindole scaffold to generate compounds that strongly compete with p53 and tightly bind to MDM2 with binding constants in the nM range [15]. Many efforts toward the development of potent non-peptide inhibitors that target the MDM2–p53 interaction are still in progress.

* Corresponding author. Tel.: +86 0411 84379593; fax: +86 0411 84675584.
E-mail address: ghli@dicp.ac.cn (G. Li).

1093-3263/$ – see front matter © 2011 Elsevier Inc. All rights reserved.
doi:10.1016/j.jmgm.2011.06.003

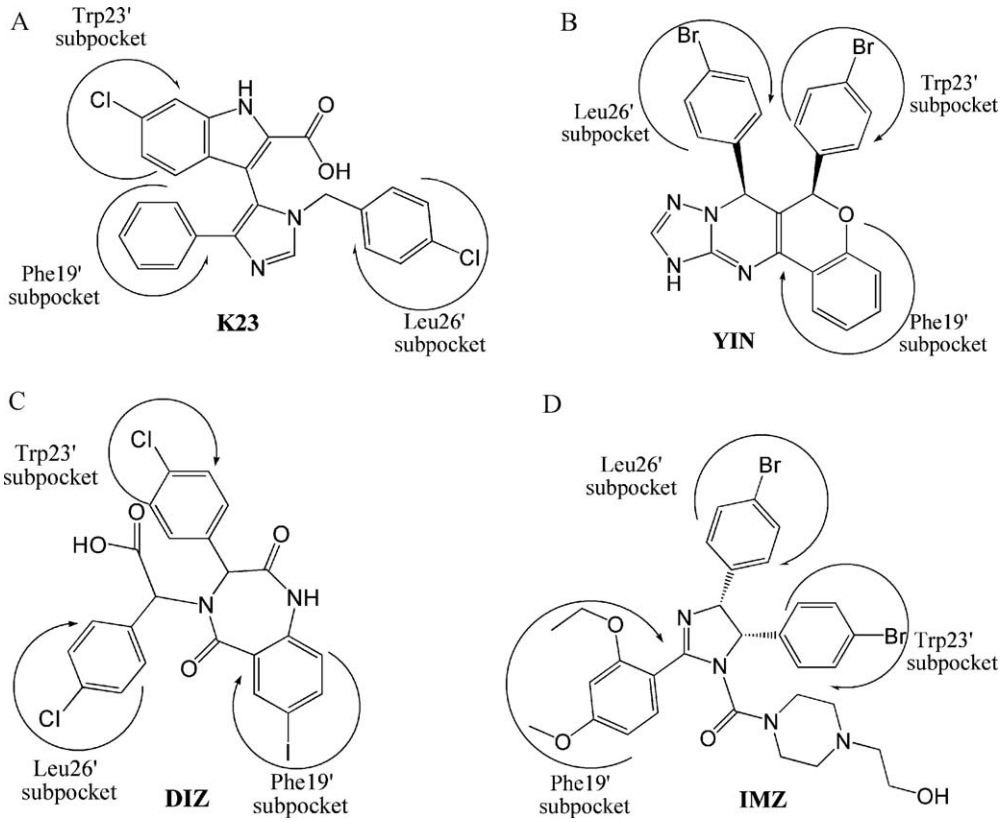

Fig. 1. Molecular structures of the four inhibitors K23 (A), YIN (B), DIZ (C) and IMZ (D). The three subpockets correspond to the hydrophobic pockets to which Phe19′, Trp23′ and Leu26′ of p53 bind, respectively.

Understanding the binding mechanisms of these small molecules to MDM2 at the atomic level may facilitate the development of potent non-peptide inhibitors that disrupt the MDM2–p53 interaction and provide valuable information about the structure–affinity relationships of the four current inhibitor-MDM2 complexes. A few computational studies have been performed for this purpose. The results from G. Zhang et al. showed that van der Waals energies are the largest component of the binding free energy for the inhibitor-MDM2 complex [19]. C. Verma et al. used molecular dynamics simulations to explore the differences between the binding of p53 and nutlin to MDM2/MDMX [20]. The studies of H.A. Carlson et al. suggested that an additional hydrophobic pocket in the interior of MDM2 should possibly be used to design new inhibitors [21]. In this work, we selected four non-peptide small molecules, DIZ [22], YIN [5], IMZ [1] and K23 [15] (Fig. 1), to explore the mechanisms of inhibition of the interaction of p53 with MDM2. The structural basis of designing these molecules relies on the interaction modes mediated by three hydrophobic residues (Phe19′, Trp23′ and Leu26′) of p53 and a deep hydrophobic cleft in MDM2; the parts of the four inhibitors that correspond to Phe19′, Trp23′ and Leu26′ of p53 are displayed in Fig. 1.

Binding free energy calculations and analyses have been shown to be powerful and valuable tools for understanding the mechanisms of interaction between small molecules and their targets. Several effective methods have been proposed for calculation of the binding free energies of protein inhibitors: free energy perturbation (FEP) [23], thermodynamic integration (TI) [24] and MM-GB/SA [25–34]. Although FEP and TI should give more accurate binding free energies, they are restricted to closely related chemical structures of small molecules. Thus, the MM-GB/SA method combined with molecular dynamics (MD) simulation was adopted to study the interaction mechanisms of the selected four small molecules with MDM2. The results show that intensive van der Waals interactions drive binding of the four inhibitors to MDM2. Furthermore, the hydrophobic contacts between the inhibitors and individual residues of MDM2 along the MD simulation were analyzed using the LIGPLOT 4.2 program [35], and the detailed van der Waals energies between these four inhibitors and individual MDM2 residues were calculated using a per-residue-based decomposition method [36]. Analyses from the two methods revealed similar binding modes for the four inhibitors to MDM2 and provide useful insights into the mechanisms of inhibition of the MDM2–p53 interaction. In addition, the effects of the inhibitors on the dynamics of the protein were analyzed. We expect that this study will provide important hints for the design of non-peptide small molecules to efficiently treat cancers caused by defects in p53 function.

2. Theory and Method

2.1. System preparation

Four X-ray structures selected from the Protein Data Bank (PDB) were studied in this work: 1T4E for MDM2-DIZ [22], 3JZK for MDM2-YIN [5], 1RV1 for MDM2-IMZ [1] and 3LBK for MDM2-K23 [15]. Due to the difference in the lengths of the protein sequences, only residues 26–109 were used for our simulation. Furthermore, the amino terminus Thr26 and the carbonyl terminus Val109 were capped by an acetyl group (ACE) and an N-methyl group (NME), respectively. All of the missing hydrogen atoms in MDM2 were added with the leap module in the Amber10 software package [37]. All of the crystal water molecules in the MDM2-inhibitor complex were maintained in the starting model. The ff99SB force field was applied to produce the force field parameters for the protein and crystal water molecules. The structures of the four inhibitors were minimized at the semiempirical AM1 level, and AM1-BCC charges were assigned to these inhibitors by the AM1-BCC program

in Amber. The general Amber force field (GAFF) was used to obtain the force field parameters for the four inhibitors, including the Lennard–Jones, torsion, and angle terms [38]. An appropriate number of chloride counterions were placed in the four MDM2-inhibitor complexes to neutralize the charges of the systems. Finally, the whole system was solvated in an octahedral periodic box of TIP3P water molecules, and the distance between the edges of the water box and the closest atom of the solutes was at least 10 Å [39].

2.2. Molecular dynamics simulation

To remove the bad contacts between the complex and solvent molecules, three stepwise rounds of minimization were applied to the whole system, in which harmonic constraints were applied to all non-hydrogen atoms of the complex with strengths of 50, 10 and 0 kcal mol^{-1} Å^{-2} for the first, second and third rounds, respectively. Each round consisted of a 2000-step steepest descent and a 3000-step conjugated gradient minimization. The system was heated from 0 to 300 K in 100 ps and equilibrated at 300 K for another 100 ps. After minimization and heating, a 10-ns MD simulation without restriction was carried out at a constant temperature of 300 K and a constant pressure of 1 atm to relax the system. Finally, the root-mean-square deviation (RMSD) of the MDM2 backbone atoms was computed along the MD trajectory relative to the initial structures to determine the stability of the system.

During the minimization, heating and MD simulation, particle mesh Ewald (PME) was applied to treat the long-range electrostatic interactions with a periodic boundary condition [40]. The Langevin dynamics with a collision frequency of 2.0 ps^{-1} was adopted to control the temperature of the system. The time step for all MD simulations was 2 fs, with a direct-space, non-bonded cutoff of 10 Å. The SHAKE method was used to restrict the hydrogen atoms. Initial velocities were assigned from a Maxwellian distribution at the initial temperature [41].

2.3. MM-GBSA calculation

For each complex, 100 snapshots were extracted from the last 2 ns along the MD trajectory at an interval of 20 ps. The MM-GB/SA method and the nmode module, which were implemented in Amber 10, were performed to compute the binding free energies of the four inhibitors to MDM2. In this method, the binding free energy (ΔG) can be represented as:

$$\nabla G = \Delta E_{MM} + \Delta G_{sol} - T\Delta S \quad (1)$$

where ΔE_{MM} is the difference in molecular mechanics energy between the complex and each binding partner in the gas phase, ΔG_{sol} is the solvation free energy contribution to binding and $T\Delta S$ is the contribution of entropy changes to the binding free energy. ΔE_{MM} is further divided into two parts:

$$\Delta E_{MM} = \Delta E_{ele} + \Delta E_{vdw} \quad (2)$$

where ΔE_{ele} and ΔE_{vdw} are described as the electrostatic interaction and van der Waals energy in the gas phase, respectively. The solvation free energy is expressed as:

$$\Delta G_{sol} = \Delta G_{gb} + \Delta G_{np} \quad (3)$$

where ΔG_{gb} and ΔG_{np} are the polar and non-polar contributions to the solvation free energy, respectively. The former component was computed using the pbsa program in Amber. The dielectric constants for the solute and solvent were set to 1.0 and 80.0 in the solvent in our calculations. The latter term was calculated by:

$$\Delta G_{np} = \gamma SASA + \beta \quad (4)$$

where SASA is the solvent accessible surface area and was computed using the MSMS program [42]. In this study, the values for γ and β were set to 0.0072 kcal mol^{-1} Å^{-2} and 0 kcal mol^{-1}.

The contribution of the entropy change ($T\Delta S$) to the binding free energy arises from changes in the translational, rotational and vibrational degrees of freedom. Because the contributions from translation and rotation are much smaller than vibration, $T\Delta S$ is generally calculated using classical statistical thermodynamics and normal-mode analysis. Because entropy calculations for large systems are extremely time consuming, we applied only 25 snapshots taken at an interval of 80 ps from the final 2 ns of the MD simulation to calculate the entropy contribution.

2.4. Calculation of the inhibitor–residue interaction

The inhibitor–residue interaction, which is valuable to qualitatively define the binding mechanisms of the four inhibitors to MDM2, was analyzed using a per-residue-based decomposition method and approximated by:

$$\Delta G_{inhibitor-residue} = \Delta G_{vdw} + \Delta G_{ele} + \Delta G_{gb} + \Delta G_{surf} \quad (5)$$

where ΔG_{vdw} and ΔG_{ele} are non-bonded van der Waals interactions and electrostatic interactions, respectively, between the inhibitor and each MDM2 residue in the gas phase and ΔG_{gb} and ΔG_{surf} are the polar and non-polar contributions to the inhibitor–residue interaction, respectively, the calculations of which are similar to ΔG_{gb} and ΔG_{np} in Eqs. (3) and (4). At the same time, the program LIGPLOT version 4.4.2 [35] was applied to calculate the hydrogen bond and hydrophobic interactions between the inhibitor and MDM2 protein.

2.5. Cross-correlation analysis

To investigate the extent of correlation motions caused by formation of the four inhibitor-MDM2 complexes, the cross-correlation matrix, C_{ij}, which reflects the fluctuations in the coordinates of the C_α atoms relative to their average positions from the last 2 ns of the simulations, was determined by the following equation:

$$C(i,j) = \frac{< \Delta r_i \times \Delta r_j >}{(< \Delta r_i^2 >< \Delta r_j^2 >)^{1/2}} \quad (6)$$

where the angle bracket represents an average over the sampled period and Δr_i indicates the deviation of the C_α atom of the ith residue from its mean position [43]. The value of C_{ij} fluctuates from −1 to 1. Positive C_{ij} values represent a correlated motion between the ith residue and the jth residue, while negative C_{ij} values describe an anticorrelated motion.

3. Results and discussion

3.1. Dynamic stability from MD

In this study, 10 ns MD simulations were run successfully for the four systems. To evaluate the reliable stability of the MD trajectories and the differences in the stabilities of the MD simulations, the RMSD values of the MDM2 backbone atoms relative to the initial minimized structure through the phase of the simulation were calculated (plotted in Fig. 2). One can see that the K23- and DIZ-MDM2 complexes reached equilibrium after 4 ns of the simulation phase, while the YIN- and IMZ-MDM2 complexes were not stable until about 6 ns. According to Fig. 2, the RMSD values of the K23-, DIZ-, YIN- and IMZ-MDM2 complexes were 0.80, 1.23, 1.37 and 1.39 Å, respectively, with a deviation lower than 0.67 Å; among these structures, the K23-MDM2 complex had the most reliable

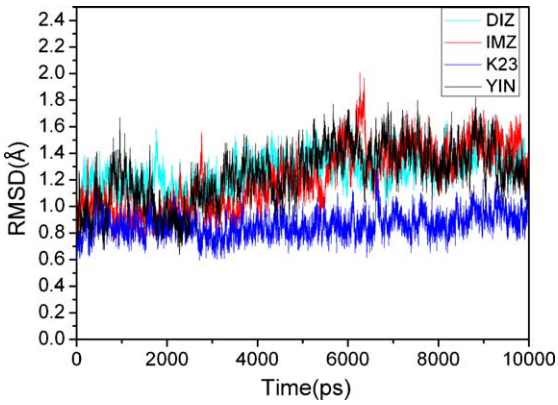

Fig. 2. The root-mean-square deviations (RMSD) of the backbone atoms relative to their initial minimized complex structures as a function of time for K23 (blue), YIN (black), DIZ (cyan) and IMZ (red). (For interpretation of the references to color in this figure legend, the reader is referred to the web version of the article.)

stability. This result shows that the trajectories of the MD simulations for the four complexes after equilibrium were reliable for post analyses.

3.2. Cross-correlation analysis

To study the effect of inhibitor binding on the dynamics of MDM2 during the simulations, cross-correlation matrices of the fluctuations were calculated and plotted in Fig. 3. The extent of correlation or anticorrelation in the movements between specific residues is displayed in a color-coded manner. By comparing Fig. 3(A–D), the changes in the internal motions induced by inhibitor binding are obvious. Overall, the presence of the four inhibitors induced pronounced anticorrelation motions (blue, dark blue), except for some moderate positive correlation movements (yellow, light red).

In the case of the K23-MDM2 complex, we noted obvious anticorrelated motions in the S2 and S3 subunits. At the same time, strong anticorrelated motions in the intersubunits (off-diagonal subunits) were also observed between the S1 and S4 subunits and the S2 and S4 subunits. Additionally, K23-MDM2 binding induced weak intrasubunit correlated motions within subunits S1 and S2.

In comparison with K23 (Fig. 3A), the presence of YIN, DIZ and IMZ generally decreased the extent of intrasubunit anticorrelated motions in the S2 and S3 subunits. Intersubunit anticorrelated motions are also reduced between the S1 and S4 subunits and the S2 and S4 subunits. However, IMZ binding increased the anticorrelated motions within the S4 subunit. In addition, correlated motion was somewhat increased by YIN binding within the S1 and S2 subunits. It is notable that the presence of DIZ and IMZ increased not only the intrasubunit correlated motions within four diagonal squares but also the intersubunit correlated motions between the S3 and S4 subunits.

The cross-correlation analysis suggests that the internal motions in the MDM2 protein are significantly affected by inhibitor binding. The differences in the motions reflect the redistribution of the residues due to the presence of the different structural inhibitors.

3.3. MM-GBSA calculation

To explore the inhibition mechanisms of the four small molecules on the MDM2–p53 interaction at the atomic level, the

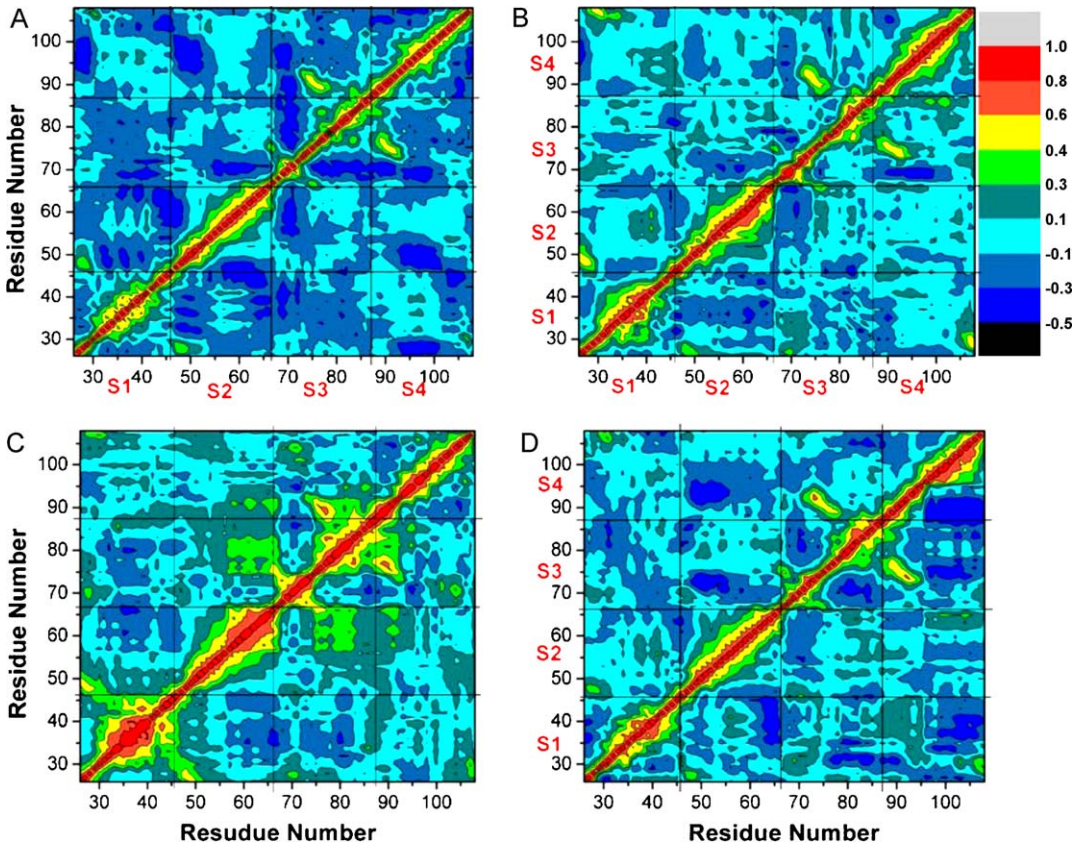

Fig. 3. Cross-correlation matrices of the fluctuations of the coordinates for C_α atoms around their mean positions during the last 2 ns of the simulations. The extent of correlated motions and anticorrelated motions are color-coded for K23 (A), YIN (B), DIZ (C) and IMZ (D).

Table 1
Binding free energy components for the protein-inhibitor complexes determined using the MM-GBSA method.[a]

Snapshot	Inhibitor	ΔE_{ele}	ΔE_{vdw}	ΔG_{np}	ΔG_{gb}	ΔG_{gbele}[b]	ΔG_{tol}[c]	$-T\Delta S$	ΔG[d]	IC50[e]
100	IMZ	−13.17 ± 2.13	−43.12 ± 2.57	−6.35 ± 0.20	24.54 ± 2.01	11.37 ± 1.72	−38.09 ± 2.21	22.50	−15.59	−9.37
	DIZ	−4.83 ± 0.48	−45.50 ± 2.45	−6.27 ± 0.18	20.04 ± 1.78	15.20 ± 1.56	−36.56 ± 1.61	20.93	−15.63	−8.72
	YIN	−6.64 ± 0.67	−37.55 ± 2.01	−5.25 ± 0.21	15.09 ± 1.64	8.45 ± 0.73	−34.36 ± 1.43	20.15	−14.21	−8.01
	K23	−1.52 ± 0.43	−39.34 ± 2.11	−5.37 ± 0.16	11.44 ± 0.84	9.92 ± 0.76	−33.27 ± 1.35	20.78	−12.49	−7.89

[a] All energies are in kcal mol^{-1}.
[b] $\Delta G_{gbele} = \Delta E_{ele} + \Delta G_{gb}$.
[c] $\Delta G_{tol} = \Delta E_{ele} + \Delta G_{gb} + \Delta G_{np} + \Delta G_{gb}$.
[d] $\Delta G = \Delta E_{ele} + \Delta G_{gb} + \Delta G_{np} + \Delta G_{gb} - T\Delta S$.
[e] The experimental values ΔG_{exp} were derived from the experimental IC50 values in Refs. [1,5,15,22] using the equation $\Delta G \approx -RT \ln TC50$.

MM-GBSA method using a single trajectory scheme was carried out to calculate the binding free energies of K23, DIZ, YIN and IMZ with MDM2. A total of 100 snapshots were taken at a time interval of 20 ps from the last 2 ns of the MD simulation for analyses of the binding free energies. Because the radius parameters of the fluorine, chlorine, bromine and iodine atoms are missing in the MM-GBSA module in Amber 10, we added radii of 1.39 Å for fluorine, 1.75 Å for chlorine, 1.85 Å for bromine and 1.98 Å for iodine to the pbsa program in Amber [44]. Table 1 lists the components of the molecular mechanics and solvation energies computed by MM-GBSA and the entropy contributions from the normal mode analysis. As seen in Table 1, the binding free energies of IMZ, DIZ, YIN and K23 to MDM2 were −15.59, −15.63, −14.21 and −12.49 kcal mol^{-1}, respectively. Furthermore, it is encouraging that the ranking of the experimental binding free energies is consistent with our predictions, which shows that the current analysis by MM-GBSA is reliable.

According to the energy components of the binding free energies listed in Table 1, the major favorable contributors to inhibitor binding were van der Waals energies (ΔE_{vdw}). Non-polar solvation energies (ΔG_{np}), which correspond to the burial of SASA upon binding, also provided important contributions to binding. However, the contributions of entropy changes ($-T\Delta S$) to the free energies impaired binding of the four inhibitors to MDM2. Although the electrostatic terms (ΔE_{ele}) favored inhibitor binding, these favorable contributions were completely screened by the unfavorable stronger polar solvation energies (ΔG_{gb}). Furthermore, it should be noted that ΔE_{vdw} is almost seven times stronger than ΔG_{np}. Therefore, van der Waals energies mostly drive binding of the four inhibitors to MDM2, which agrees well with previous experimental analyses [1,5,15,19,22]. This result suggests that optimization of van der Waals interactions between inhibitors and MDM2 may lead to potent small molecule inhibitors of the MDM2–p53 interaction.

3.4. Statistical analyses of hydrophobic contacts

To qualitatively identify which residues in MDM2 make important contributions to binding, statistical analyses of the hydrophobic and hydrogen bond contacts between the inhibitors and the residues in MDM2 during the MD simulations were performed using the program LIGPLOT version 4.4.2. The results indicate that the inhibitors K23, YIN, DIZ and IMZ form stable hydrophobic contacts with some residues of MDM2, but hydrogen

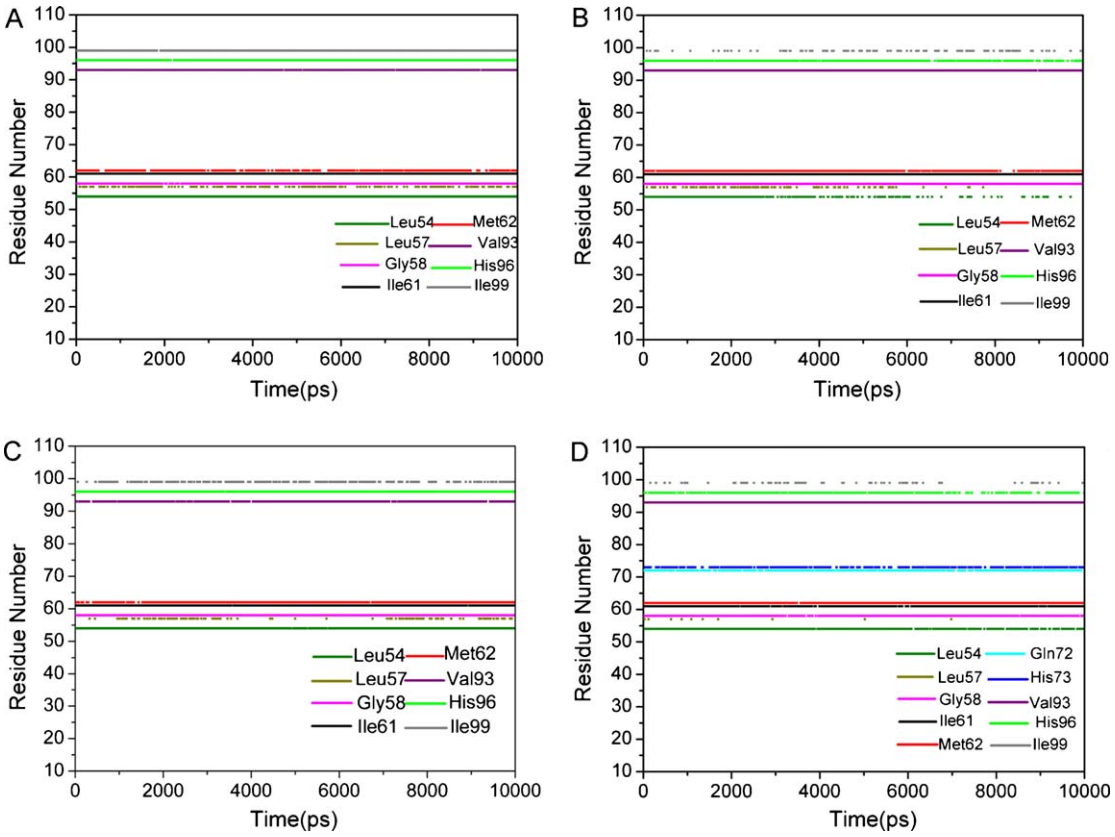

Fig. 4. The hydrophobic contacts as a function of the simulation time for K23 (A), YIN (B), DIZ (C) and IMZ (D).

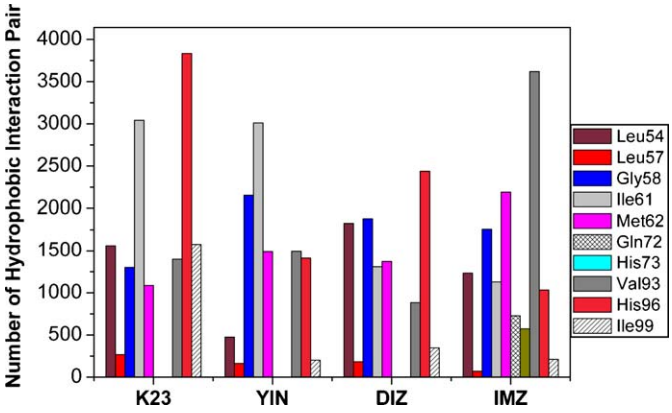

Fig. 5. The numbers of hydrophobic interaction pairs between the inhibitors and the residues of MDM2 (6–10 ns).

bond contacts between the inhibitors and MDM2 were not observed.

Fig. 4 shows plots of the hydrophobic contacts as a function of the simulation time for the K23-, YIN-, DIZ- and IMZ-MDM2 complexes. Furthermore, Fig. 5 gives the numbers of hydrophobic interaction pairs between the inhibitors and the residues of MDM2 during the last 2 ns of the MD simulation. According to Fig. 4, the four inhibitors DIZ, IMZ, YIN and K23 bind to MDM2 with a similar hydrophobic contact mode. Eight common residues, Leu54, Leu57, Gly58, Ile61, Met62, Val93, His96 and Ile99, were involved in the hydrophobic contacts, and Gln72 and His73 were also involved in the hydrophobic contacts for the inhibitor IMZ. Statistical analyses from Fig. 5 demonstrate that the four inhibitors produce stable hydrophobic interactions with six residues, Leu54, Gly58, Ile61, Met62, Val93 and His96, with hydrophobic interaction pairs higher than 470; in addition, IMZ stably contacts Gln72 and His73, and K23 interacts with Ile99. These residues form the three subpockets listed in Fig. 1. The above analyses agree with previous studies [1,5,15,19,45]. Optimization of the hydrophobic interactions of these residues with inhibitors should play a key role in the development of new potent non-peptide inhibitors of the MDM2–p53 interaction.

3.5. Analyses of the structure–affinity relationship

Because the electrostatic interaction in the gas phase is screened by the polar solvation energy, the polar term (ΔG_{gbele}) does not provide a favorable contribution to the binding (Table 1); thus, the van der Waals interactions of K23, YIN, DIZ and IMZ with individual residues in MDM2 were calculated using a per-residue-based decomposition method (Fig. 6) to obtain more detailed insight into the inhibitory mechanisms of the four inhibitors to the MDM2–p53 interaction at the atomic level. At the same time, analyses of the structure and binding mode were carried out. In Fig. 7, the relative geometries of the four inhibitors in the binding complexes with the relevant residues are plotted according the lowest-energy structure from the MD trajectory.

As seen in Fig. 6, the current inhibitors overall produce van der Waals interactions of higher than 1.0 kcal mol^{-1} with four common residues, Leu54, Gly58, Ile61 and Val93, which reflects similar binding modes. However, the van der Waals interactions of IMZ with Gln72 and His73 also exceeded 1.0 kcal mol^{-1}, which indicates that the structures of the four small molecules are different (Fig. 1).

According to Fig. 6A, six residues are involved in the main binding attractions, with van der Waals interactions stronger than 1 kcal mol^{-1} for the MDM2-K23 complex. The van der Waals ener-

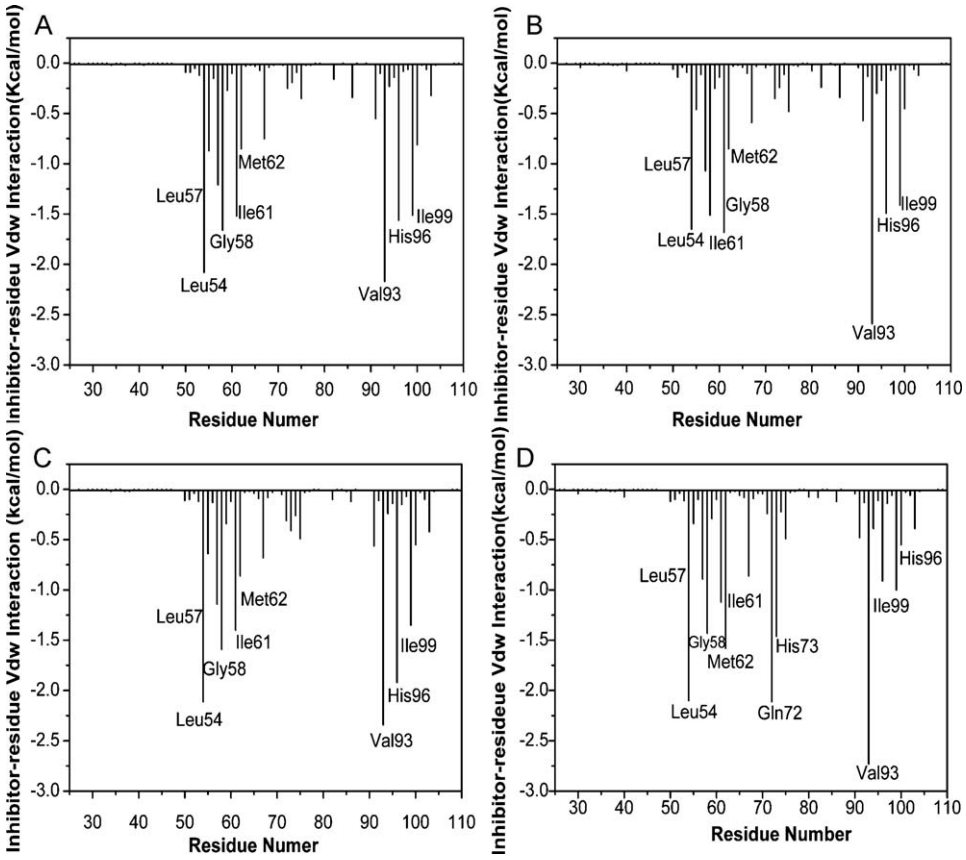

Fig. 6. The Van der Waals interactions between the inhibitors, K23 (A), YIN (B), DIZ (C) and IMZ (D), and the residues of MDM2.

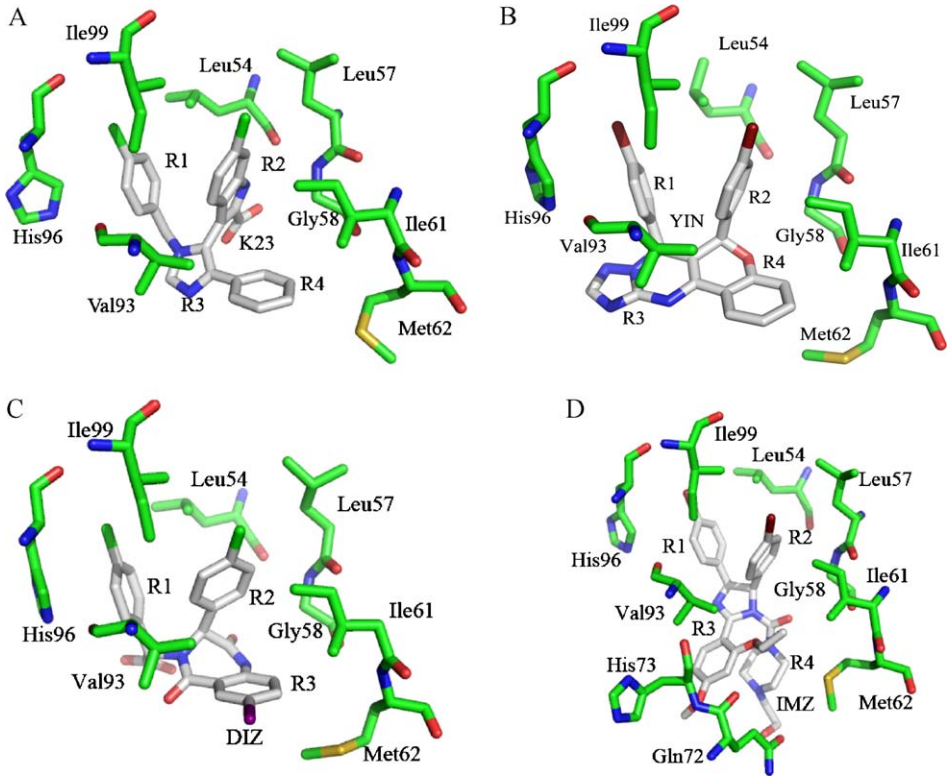

Fig. 7. Geometries of key residues that produce favorable interactions with the four inhibitors are modeled in the complexes according to the lowest-energy structure from the MD trajectory for K23 (A), YIN (B), DIZ (C) and IMZ (D).

gies that drive the binding of K23 to Leu54 and His96 were −2.08 and −1.56 kcal mol^{-1}, respectively. These two driving forces were mainly caused by insertion of the R1 ring of K23 into the hydrophobic cleft in MDM2 (Fig. 7A) formed by Leu54 and His96. In this cleft (corresponding to the Leu26′ subpocket in Fig. 1A), the imidazole ring of His96 and the R1 ring of K23 form a T-shaped-like π–π interaction [46], while the alkyl moiety of Leu54 makes CH–π contacts with the R1 ring of K23. The alkyl groups of Leu57 and Ile99 and the CH groups of Gly58 generate a number of CH–π contacts with the chlorine-substituted indole ring (R2) of K23, which results in van der Waals energies of −1.21, −1.66 and −1.51 kcal mol^{-1} for Leu57, Gly58 and Ile99 (Fig. 6A), respectively. These three residues form the second hydrophobic cleft (corresponding to the Trp23′ subpocket) to which the R2 ring of K23 binds. Among the residues Ile61, Met62 and Val93 that form the Phe19′ subpocket in Fig. 1A, the alkyl group of Val93 forms the most CH–π contacts with the imidazole ring (R3) and benzene group (R4) of K23, and there are less CH–π contacts between the alkyl moiety of Ile61 and the benzene group (R4) of K23 compared with Val93. Met62 makes the least number of CH–π contacts with the R4 ring of K23 (Figs. 4A, 5 and 7A). This result agrees with the rank of the van der Waal energies of −2.17, −1.62 and −0.85 kcal mol^{-1} for Val93, Ile61 and Met62, respectively. The above analyses are also consistent with previous statistical analyses and other studies [1,5,15,19,22].

As seen in Figs. 6 and 7, the inhibitors YIN, DIZ and IMZ bind to MDM2 in a mode similar to K23. The R1, R2 and R3(R4) rings of these three inhibitors also insert into three hydrophobic subpockets (Fig. 1) to produce favorable CH–π and π–π contacts. Thus, the binding analyses of YIN, DIZ and IMZ to MDM2 are almost the same as K23.

From Fig. 7D, the R1 ring of IMZ also generates a T-shaped-like π–π interaction with the imidazole ring of His96; however, a nearly parallel π–π interaction occurred between the imidazole ring of His96 and the R1 rings of YIN and DIZ (Fig. 7B and C). In addition, Gln72 also formed some advantageous CH–π contacts with the R3 and R4 rings of IMZ (Fig. 7D), which leads to a van der Waals energy of −2.11 kcal mol^{-1} (Fig. 6D), while the van der Waals energy of −1.46 kcal mol^{-1} resulted from a weak π–π interaction between the R3 ring of IMZ and the imidazole ring of His73 and several CH–π contacts (Figs. 6D and 7D). To summarize, the CH–π interactions and π–π interactions between individual residues of MDM2 and the inhibitors drive binding of K23, YIN, DIZ and IMZ to MDM2.

4. Conclusions

In this work, 10 ns MD simulations and calculations of binding free energies using the MM-GBSA method were performed to study the binding of four small molecule inhibitors to MDM2, and the results show that van der Waals energies in the gas phase drive binding of the inhibitors to MDM2. Analyses of the hydrophobic contacts suggest that the four inhibitors form stable hydrophobic interactions with the residues Leu54, Gly58, Ile61, Met62, Val93 and His96, and these hydrophobic interactions also play a key role in binding. Analyses of the detailed van der Waals interactions show that the CH–π and π–π interactions between the four inhibitors and residues of MDM2 drive binding of the inhibitors in the hydrophobic cleft of MDM2. Thus, optimization of the CH–π and π–π interactions between the hydrophobic groups of the inhibitors and the protein residues may lead to potent non-peptide small molecule inhibitors that target the MDM2–p53 interaction.

Acknowledgments

This work is supported by the National High-tech Research and Development Program (2009AA01A137), the National Natural Science Foundation of China (31070641/C050101) and “Hundred Talents Program of the Chinese Academy Sciences”.

References

[1] L.T. Vassilev, B.T. Vu, B. Graves, D. Carvajal, F. Podlaski, Z. Filipovic, N. Kong, U. Kammlott, C. Lukacs, C. Klein, N. Fotouhi, E.A. Liu, In vivo activation of the p53 pathway by small-molecule antagonists of MDM2, Science 303 (2004) 844–848.

[2] B. Vogelstein, D. Lane, A.J. Levine, The p53 tumour-suppressor gene integrates numerous signals that control cell life and death, as when a highly connected node in the Internet breaks down, the disruption of p53 has severe consequences, Nature 408 (2000) 307–310.

[3] A.J. Levine, P53, the cellular gatekeeper for growth and division, Cell 88 (1997) 323–331.

[4] A.S. Dudkina, C.W. Lindsley, Small molecule protein–protein inhibitors for the p53–MDM2 interaction, Curr. Top. Med. Chem. 7 (2007) 952–960.

[5] J.G. Allen, M.P. Bourbeau, G.E. Wohlhieter, M.D. Bartberger, K. Michelsen, R. Hungate, R.C. Gadwood, R.D. Gaston, B. Evans, L.W. Mann, M.E. Matison, S. Schneider, X. Huang, D. Yu, P.S. Andrews, A. Reichelt, A.M. Long, P. Yakowec, E.Y. Yang, T.A. Lee, J.D. Oliner, Discovery and optimization of chromenotriazolopyrimidines as potent inhibitors of the mouse double minute 2-tumor protein 53 protein–protein interaction, J. Med. Chem. 52 (2009) 7044–7053.

[6] A.D. Bautista, J.S. Appelbaum, C.J. Craig, J. Michel, A. Schepartz, Bridged β^3-Peptide Inhibitors of p53–hDM2 complexation: correlation between affinity and cell permeability, J. Am. Chem. Soc. 132 (2010) 2904–2906.

[7] R. Fasan, R.L.A. Dias, K. Moehle, O. Zerbe, J.W. Vrijbloed, D. Obrecht, J.A. Robinson, Using a ß-hairpin to mimic an alpha-helix-Novel cyclic peptidomimetic inhibitors of the p53–HDM2 protein–protein interaction, Angew. Chem. Int. Ed. 43 (2004) 2109–2112.

[8] J.A. Kritzer, J.D. Lear, M.E. Hodsdon, A. Schepartz, Helical α-peptide inhibitors of the p53–hDM2 interaction, J. Am. Chem. Soc. 126 (2004) 9468–9469.

[9] R. Stoll, C. Renner, S. Hansen, S. Palme, C. Klein, A. Belling, W. Zeslawski, M. Kamionka, T. Rehm, P. Muhlhahn, R. Schumacher, F. Hesse, B. Kaluza, W. Voelter, R.A. Engh, T.A. Holak, Chalcone derivatives antagonize interactions between the human oncoprotein MDM2 and p53, Biochemistry 40 (2001) 336–344.

[10] J. Zhao, M. Wang, J. Chen, A. Luo, X. Wang, M. Wu, D. Yin, Z. Liu, The initial evaluation of non-peptidic small-molecule HDM2 inhibitors based on p53–HDM2 complex structure, Cancer. Lett. 183 (2002) 69–77.

[11] L.T. Vassilev, P53 activation by small molecules: application in oncology, J. Med. Chem. 48 (2005) 4491–4703.

[12] K. Ding, Y. Lu, Z. Nikolovska-Koleska, S. Qiu, Y. Ding, W. Gao, J. Stuckey, P.P. Roller, Y. Tomita, J.R. Deschamps, S. Wang, Structure-based design of potent non-peptide MDM2 inhibitors, J. Am. Chem. Soc. 127 (2005) 10130–10131.

[13] H. Yin, G.I. Lee, H.S. Park, G.A. Payne, J.M. Rodriguez, Terphenyl-based helical mimetics that disrupt the p53–HDM2 interaction, Angew. Chem. Int. Ed. 44 (2005) 2704–2710.

[14] P. Chene, Inhibiting the p53–MDM2 interaction: an important target for cancer therapy, Nat. Rev. Cancer. 2 (2003) 102–109.

[15] G.M. Popowicz, A. Czarna, S. Wolf, K. Wang, W. Wang, A. Döling, T.A. Holak, Structure of low molecular weight inhibitors bound to MDMX and MDM2 reveal new approaches for p53–MDMX/MDM2 antagonist drug discovery, Cell. Cycle 9 (2010) 1104–1111.

[16] H.K. Koblish, S. Zhao, C.F. Franks, R.R. Donatelli, R.M. Tominovich, L.V. LaFrance, K.A. Leonard, J.M. Gushue, D.J. Parks, R.R. Calvo, K.L. Milkiewicz, J.J. Marugán, P. Raboisson, M.D. Cummings, B.L. Grasberger, D.L. Johnson, T. Lu, C.J. Molloy, A.C. Maroney, Benzodiazepinedione inhibitors of the Hdm2: p53 complex suppress human tumor cell proliferation in vitro and sensitize tumors to doxorubicin in vivo, Mol. Cancer. Therap. 5 (2006) 160–169.

[17] S. Shangary, S.M. Wang, Targeting the MDM2–p53 interaction for cancer therapy, Clin. Cance. Res. 14 (2008) 5318–5324.

[18] S. Shangary, S.M. Wang, Small-molecule inhibitors of the MDM2–p53 protein–protein interaction to reactivate p53 function: a novel approach for cancer therapy, Annu. Rev. Pharmacol. Toxicol. 49 (2009) 223–241.

[19] G. Hu, D. Wang, X. Liu, Q. Zhang, A computational analysis of the binding model of MDM2 with inhibitors, J. Comp. Aid. Mol. Des. 24 (2010) 687–697.

[20] T. Leonard, J. Arumugam, M. Christopher, J. Brown, D.P. Lane, C. Verma, Differential binding of p53 and nutlin to MDM2 and MDMX: computational studies, Cell. Cycle 9 (2010) 1167–1181.

[21] H. Zhong, H.A. Carlson, Computational studies and peptidomimetic design for the human p53–MDM2 complex, Proteins 58 (2005) 222–234.

[22] B.L. Grasberger, T. Lu, C. Schubert, D.J. Parks, T.E. Carver, H.K. Koblish, D. Cummings Maxwell, L.V. LaFrance, L. Milkiewicz Karen, R.R. Calvo, D. Maguire, J. Lattanze, C.F. Franks, S. Zhao, K. Ramachandren, G.R. Bylebyl, M. Zhang, C.L. Manthey, E.C. Petrella, M.W. Pantoliano, I.C. Deckman, J.C. Spurlino, A.C. Maroney, B.E. Tomczuk, C.J. Molloy, R.F. Bone, Discovery and cocrystal structure of benzodiazepinedione HDM2 antagonists that activate p53 in cells, J. Med. Chem. 48 (2005) 909–912.

[23] P.L. Cummins, J.E. Gready, Computer-aided drug design: a free energy perturbation study on the binding of methyl-substituted pterins and N5-deazapterins to dihydrofolate reductase, J. Comput. Aid. Mol. Des. 7 (1993) 535–555.

[24] T. Simonson, J. Carlsson, D.A. Case, Proton binding to proteins: pKa calculations with explicit and implicit solvent models, J. Am. Chem. Soc. 126 (2004) 4167–4180.

[25] Y. Tong, Y. Mei, Y.L. Li, C.C. Ji, J.Z.H. Zhang, Electrostatic polarization makes a substantial contribution to the free energy of avidin–biotin binding, J. Am. Chem. Soc. 132 (2010) 5137–5142.

[26] J. Chen, S. Zhang, X. Liu, Q. Zhang, Insights into drug resistance of mutations D30N and I50V to HIV-1 protease inhibitor TMC-114: free energy calculation and molecular dynamic simulation, J. Mol. Model. 16 (2010) 459–468.

[27] E.L. Wu, K.L. Han, J.Z.H. Zhang, Selectivity of neutral/weakly basic P1 group I inhibitors of thrombin and trypsin by a molecular dynamics study, Chem. Eur. J. 14 (2008) 8704–8714.

[28] T. Hou, R. Yu, Molecular dynamics and free energy studies on the wild-type and double mutant HIV-1 protease complexed with amprenavir and two amprenavir-related inhibitors: mechanism for binding and drug resistance, J. Med. Chem. 50 (2007) 1177–1188.

[29] Y. Xu, R. Wang, A computational analysis of the binding affinities of FKBP12 inhibitors using the MM-PB/SA method, Proteins 64 (2006) 1058–1068.

[30] B. Kuhn, P. Gerber, T. Schulz-Gasch, M. Stahl, Validation and use of the MM-PBSA approach for drug discovery, J. Med. Chem. 48 (2005) 4040–4048.

[31] W. Wang, W.A. Lim, A. Jakalian, J. Wang, R. Luo, C.I. Bayly, P.A. Kollman, An analysis of the interactions between the sem-5 SH3 domain and its Ligands using molecular dynamics, free energy calculations, and sequence analysis, J. Am. Chem. Soc. 123 (2001) 3986–3994.

[32] W. Wang, P.A. Kollman, Free energy calculations on dimer stability of the HIV protease using molecular dynamics and a continuum solvent model, J. Mol. Biol. 303 (2000) 567–582.

[33] J. Wang, P. Morin, W. Wang, P.A. Kollman, Use of MM-PBSA in reproducing the binding free energies to HIV-1 RT of TIBO derivatives and predicting the binding Mode to HIV-1 RT of efavirenz by docking and MM-PBSA, J. Am. Chem. Soc. 123 (2001) 5221–5230.

[34] J.M. Swanson, R.H. Henchman, J.A. McCammon, Revisiting free energy calculations: a theoretical connection to MM/PBSA and direct calculation of the association free energy, Biophys. J. 86 (2004) 67–74.

[35] A.C. Wallace, R.A. Laskowski, J.M. Thornton, LIGPLOT: a program to generate schematic diagrams of protein–ligand interactions, Protein Eng. 8 (1995) 127–134.

[36] H. Gohlke, C. Kiel, D.A. Case, Insights into protein–protein binding by binding free energy calculation and free energy decomposition for the Ras–Raf and Ras–RalGDS complexes, J. Mol. Biol. 330 (2003) 891–913.

[37] D.A. Case, T.A. Darden, T.E. Cheatham, C.L. Simmerling III, J. Wang, R.E. Duke, R. Luo, M. Crowley, R.C. Walker, W. Zhang, K.M. Merz, B. Wang, S. Hayik, A. Roitberg, G. Seabra, I. Kolossváry, K.F. Wong, F. Paesani, J. Vanicek, X. Wu, S.R. Brozell, T. Steinbrecher, H. Gohlke, L. Yang, C. Tan, J. Mongan, V. Hornak, G. Cui, D.H. Mathews, M.G. Seetin. C. Sagui, V. Babin, P.A. Kollman, AMBER. 10, University of California, San Francisco, 2008.

[38] J.M. Wang, P. Gieplak, P.A. Kollman, How well does a restrained electrostatic potential (RESP) model perform in calculating conformational energies of organic and biological molecules? J. Comput. Chem. 21 (2000) 1049–1074.

[39] W.L. Jorgensen, J. Chandrasekhar, J.D. Madura, R.W. Impey, M.L. Klein, Comparison of simple potential functions for simulating liquid water, J. Chem. Phys. 79 (1983) 926–935.

[40] T. Darden, D. York, L. Pedersen, Particle mesh Ewald: an N-log (N) method for Ewald sums in large systems, J. Chem. Phys. 98 (1993) 10089–10092.

[41] J.P. Ryckaert, G. Ciccotti, H.J.C. Berendsen, Numerical integration of the cartesian equations of motion of a system with constraints: molecular dynamics of n-alkanes, J. Comput. Phys. 23 (1997) 327–341.

[42] M.F. Sanner, A.J. Olson, J. Spehner, Reduced surface: an efficient way to compute molecular surface, Biopolymers 38 (1996) 305–320.

[43] T. Ichiye, M. Karplus, Essential dynamics of proteins, Proteins 17 (1993) 412–425.

[44] K.E. Riley, K.M. Merz Jr., Insights into the strength and origin of halogen bonding: the halobenzene–formaldehyde dimmer, J. Phys. Chem. A 111 (2007) 1688–1694.

[45] Y. Ding, Y. Mei, J.Z.H. Zhang, Quantum mechanical studies of residue-specific hydrophobic interactions in p53−MDM2 binding, J. Phys. Chem. B 112 (2008) 11396–11401.

[46] Y. Ding, Y. Mei, J.Z.H. Zhang, F. Tao, Efficient bond function basis set for π–π interaction energies, J. Comput. Chem. 29 (2008) 275–279.